arXiv:0903.0672v1 [astro-ph.GA] 4 Mar 2009

Spatial Variations in Galactic H I Structure on AU-Scales Toward 3C 147 Observed with the Very Long Baseline Array

T. Joseph W. Lazio
Naval Research Laboratory, 4555 Overlook Avenue SW, Washington, DC 20375-5351
`Joseph.Lazio@nrl.navy.mil`

C. L. Brogan
National Radio Astronomy Observatory, 520 Edgemont Road, Charlottesville, VA 22903-2475

W. M. Goss
National Radio Astronomy Observatory, P. O. Box O, 1003 Lopezville Road, Socorro, NM 87801
and

Snežana Stanimirović
Department of Astronomy, University of Wisconsin, Madison, WI 53706

ABSTRACT

This paper reports dual-epoch, Very Long Baseline Array observations of H I absorption toward 3C 147. One of these epochs (2005) represents new observations while one (1998) represents the reprocessing of previous observations to obtain higher signal-to-noise results. Significant H I opacity and column density variations, both spatially and temporally, are observed with typical variations at the level of $\Delta\tau \approx 0.20$ and in some cases as large as $\Delta\tau \approx 0.70$, corresponding to column density fluctuations of order 5×10^{19} cm^{-2} for an assumed 50 K spin temperature. The typical angular scale is 15 mas; while the distance to the absorbing gas is highly uncertain, the equivalent linear scale is likely to be about 10 AU. Approximately 10% of the face of the source is covered by these opacity variations, probably implying a volume filling factor for the small-scale absorbing gas of no more than about 1%. Comparing our results with earlier results toward 3C 138 (Brogan et al.), we find numerous similarities, and we conclude that small-scale absorbing gas is a ubiquitious phenomenon, albeit with a low probability of intercept on any given line of sight. Further, we compare the volumes sampled by the line of sight through the Galaxy between our two epochs and conclude that, on the basis of the motion of the Sun alone, these two volumes are likely to be substantially different. In order to place more significant constraints on the various models for the origin of these small-scale structures, more frequent sampling is required in any future observations.

Subject headings: galaxies: individual (3C 147) — ISM: general — ISM: structure — radio lines: ISM — techniques: interferometric

1. Introduction

Beginning with a two-antenna very long baseline interferometric (VLBI) observation of 3C 147 by Dieter et al. (1976), a variety of H I absorption studies over the past three decades have found AU-scale optical depth variations in the Galactic interstellar medium (ISM). The initial detections were confirmed by Diamond et al. (1989), and the first images of the small-scale H I in the direction of 3C 138 and 3C 147 were made by Davis et al. (1996) using MERLIN. Faison et al. (1998) and Faison & Goss (2001) used the Very Long Baseline Array (VLBA) to improve the resolution toward a number of sources to approximately 20 mas ($\sim$ 10 AU). Significant variations were detected in the direction of 3C 138 and 3C 147, while no significant variations in H I opacity were found in the direction of five other compact radio sources.

An independent means of probing small-scale neutral structures is multi-epoch H I absorption measurements of high proper motion pulsars (Frail et al. 1994; Johnston et al. 2003; Stanimirović et al. 2003). While early pulsar observations suggested that small-scale structure might be ubiquitous, more recent observations suggest that it could be more sporadic. A significant advantage of VLBI observations is that they provide 2-D images of the opacity variations, rather than 1-D samples as in the case of pulsars observations.

Brogan et al. (2005) revisited the observations of 3C 138, by re-analyzing the 1995 VLBA observations (Faison et al. 1998) and by obtaining two new epochs of observations (1999 and 2002). They confirmed the initial results of Faison & Goss (2001), that there are small-scale opacity changes along the line of sight to 3C 138 at the level of $\Delta\tau_{\rm max} = 0.50 \pm 0.05$, with typical sizes of roughly 50 mas ($\sim$ 25 AU). However, with multiple epochs and improvements in data analysis techniques (yielding an increase of a factor of 5 in the sensitivity of the 1995 epoch), they reached a number of additional significant conclusions:

1. They found clear evidence for temporal variations in the H I opacity over the seven-year time span of the three epochs, consistent with structures moving across the line of sight at velocities of a few tens of kilometers per second, though the infrequent sampling in time means that they could not determine whether these structures were persistent.

2. They found no evidence for a drop in the H I spin temperature, as would be evidenced by a narrowing of line widths at small scales compared to single dish measurements. In turn, a constant H I spin temperature implies that the small-scale opacity variations are due to density enhancements, although these enhancements would necessarily be extremely over-pressured relative to the mean interstellar pressure, far from equilibrium, and likely of relatively short duration.

3. For the first time they determined that the plane of sky covering fraction of the small-scale H I gas is roughly 10%. In turn, this small covering fraction suggests that the volume filling factor of such gas, within the cold neutral medium, is quite low ($\lesssim$ 1%), in agreement with HST observations of high-pressure gas in the ISM (Jenkins & Tripp 2001; Jenkins 2004).

4. They simulated pulsar observations that have been used to search for H I opacity variations and showed that the existing pulsar observations have generally been too sparsely sampled (in time) to be useful in studying the details of small-scale H I opacity variations.

While the multi-epoch study of Brogan et al. (2005) represented a substantial improvement, nonetheless their conclusions rested on observations of only one line of sight. In light of this sample of one, their conclusions might seem rather audacious, particularly given the larger sample observed by Faison et al. (1998) and Faison & Goss (2001), in which most of the objects did not show variations in the H I absorption. The 3C 138 study has shown that the key to a successful small scale H I study is a background source with both high surface brightness ($\gtrsim$ 60 mJy beam^{-1}) and large angular extent ($>$ 100 mas). The quasar 3C 147 is one of the few sources that shares these characteristics with 3C 138. This paper presents dual-epoch observations of 3C 147 that were designed specifically to confront the conclusions of Brogan et al. (2005) with a second line of sight. Section 2 of this paper describes the observations, focussing on the new observations acquired for the second epoch, §3 discusses the results, and §4 presents our conclusions and recommendations for future work.

2. Observations

We have observed the Galactic H I absorption (near $-10\,{\rm km\ s^{-1}}$) toward the quasar 3C 147 at two epochs. Epoch I was 1998 October 22, and the results from those observations have been published previously by Faison & Goss (2001). Epoch II consists of new data observed on 2005 August 21. Table 1 summarizes the basic observing parameters for the two epochs.

For both epochs the data were obtained using the 10 antennas of the Very Long Baseline Array combined with the Very Large Array with its 27 antennas operating in a phased-array mode. For the 2005 epoch, the Green Bank Telescope was also used. The observing duration was 12 hr for the 1998 epoch and 16 hr for the 2005 epoch, including time spent on calibration sources. The proximity of the VLA to the VLBA antenna at Pie Town, New Mexico, significantly increased our sensitivity to large-scale structures. Four separate spectral windows or intermediate frequency bands (IFs) were used, with one IF centered on the absorption line (at an approximate LSR velocity of $-10\,\mathrm{km\ s^{-1}}$) and three IFs separated by at least 100 km $\mathrm{s^{-1}}$ in velocity in order to sample the 21 cm continuum emission. For the 1998 epoch, the data were correlated with velocity channels of 0.4 km $\mathrm{s^{-1}}$, with a bandwidth of 500 kHz per IF over 256 spectral channels; for the 2005 epoch, improvements in the correlator allowed the number of spectral channels per IF to be increased to 512, with a concomitant improvement in the velocity resolution to 0.2 km $\mathrm{s^{-1}}$.

Broadly similar data reduction procedures were used for the two epochs. For the 2005 epoch, the data were calibrated for the frequency dependence of the bandpass using observations of 3C 48 and amplitude calibrated using system temperatures measured at the individual antennas. The most significant difference in the calibration is that for the 2005 epoch, we attempted to phase-reference the observations to the compact source IVS B0532+506, separated by $1\overset{\circ}{.}3$ from 3C 147.

Our initial motivation for this change in procedure is that 3C 147 has a sufficiently complex structure that fringe-fitting assuming a point-source model could yield erroneous residual delay and rate solutions. In practice, phase referencing did not prove useful. The phase-referencing cycle time was short enough that latency in the VLA system often resulted in the VLA acquiring no data. The most significant difficulty, however, was that only one of the epochs was phase-referenced. There was an apparent offset in the core position between the two epochs (with a magnitude of a fraction of the synthesized beam width or a few milliarcseconds) that biased any attempt to compare results from the two epochs (e.g., comparing the integrated line profiles). Consequently, we did not make use of the phase-referenced data for constructing the H I line profile or opacity images. One obvious impact on our results is that the sensitivity of the 2005 epoch H I line data is less than it could have otherwise been due to the phase-referencing cycling between 3C 147 and IVS B0532+506.

Two of the three continuum IFs were then averaged together and several iterations of hybrid imaging (iterative imaging and self-calibration) were performed. After the final iteration of self-calibration, the phase and amplitude solutions were applied to the IF containing the H I line. The line-free velocity channels in this IF were averaged together to produce a continuum data set, which underwent a final round of hybrid imaging, the solutions from which were applied to the velocity channels containing the line. Finally, the continuum emission was subtracted from the velocity channels containing the H I line and the resulting line data set was imaged.

We also reprocessed the observations of Faison & Goss (2001) in a similar fashion. A significant difference from the original analysis of Faison & Goss (2001) is that we used the continuum image from the 2005 epoch as an initial model for fringe fitting the 1998 epoch data (for which no phase referencing was performed). The combination of a better initial model and improvements in the imaging software and analysis procedures led to a substantial improvement in the reprocessed 1998 epoch data. The noise in the 1998 epoch continuum image has improved by nearly an order of magnitude, and the improvement in the spectral line images is a factor of a few. As was the case for 3C 138, the original analysis found a significantly higher peak brightness than we do, by a similar factor ($\approx 30\%$). Like Brogan et al. (2005), we attribute this difference to the use of a point source model by Faison & Goss (2001) in the original fringe fitting along with other details of the subsequent imaging and self-calibration.

Following the procedure of Faison & Goss (2001), both the continuum images and continuum-

TABLE 1
OBSERVATIONAL LOG

Parameter	Faison & Goss (2001)	Epoch I	Epoch II
Date	1998 October 22	1998 October 22	2005 August 21
Number of IFs	4	4	4
Bandwidth per IF (MHz)	0.5	0.5	0.5
Spectral channels	256	256	512
Channel separation (km s^{-1})	0.41	0.41	0.21
Velocity resolution (km s^{-1})[a]	0.4	0.41	0.21
CLEAN beam (mas)[b]	5 × 4	8.2 × 5.6	7.6 × 7.1
Continuum Peak (Jy $beam^{-1}$)[c]	2.31	1.681	1.801
Continuum rms noise (mJy $beam^{-1}$)[c]	6.5	1.7	1.1
Spectral line rms noise (mJy $beam^{-1}$)[c]	7.6	5.0	3.5
General Parameters for 3C 147			
Position (equatorial, J2000)	$05^{\rm h}42^{\rm m}36\overset{\rm s}{.}13788$	$+49^{\circ}07'51\overset{''}{.}2335$	
Position (Galactic, longitude & latitude)	$+161.69^{\circ}$	$+10.30^{\circ}$	
Redshift	0.545		

[a] After Hanning smoothing during imaging process.

[b] The CLEAN beam before convolution to 10 mas. All subsequent values are for the convolved 10 mas resolution images.

[c] For the image after it has been convolved to 10 mas resolution.

NOTE.—The values listed under the Faison & Goss (2001) column are for the original analysis. The values listed under the Epoch I column are for this analysis, after the reprocessing of the data as described in the text.

subtracted line cubes were convolved to 10 mas resolution. The *u*-*v* coverages for the visibility data from the two epochs were similar, producing images with angular resolutions of approximately 7 mas (Table 1). The convolution of the continuum images and continuum-subtracted line cubes is an attempt to minimize any effects of modest differences in the *u*-*v* coverage between the epochs. The second epoch data were also smoothed in velocity so that their velocity resolution matched that of the first epoch.

An optical depth cube, calculated as $\tau_{H\,I}(\alpha,\delta,v) = -\ln[1 - I_{\rm line}(\alpha,\delta,v)/I_{\rm cont}(\alpha,\delta)]$, where $I_{\rm line}$ and $I_{\rm cont}$ are, respectively, the images from formed from line and line-free channels. Because the signal-to-noise ratio in the optical depth images is low where the continuum emission is weak, the optical depth images were blanked where the continuum emission was less than 5% of the peak emission.

3. Results

3.1. 21 cm Continuum

Figure 1 presents the 21 cm continuum image of 3C 147 from the new observations of the 2005 epoch. There is good qualitative agreement between our image and previously published images at comparable wavelengths (18–20 cm, Readhead & Wilkinson 1980; Zhang et al. 1991; Polatidis et al. 1995; Faison & Goss 2001). The source displays its well-known core-jet structure, with the jet extending some 200 mas to the southwest before bending to the north. Also prominent is diffuse emission to the east of the core, extending to the north, first noticed by Zhang et al. (1991). The resolution of our observations is not high enough to resolve the northeast extension from the core found by Readhead & Wilkinson (1980).

We assessed the continuum images from the two epochs for variability. Creating a difference image between the two epochs, we find that any variability in the source is below the 20 mJy beam^{-1} level. Even if the source is variable at this level, as for the Brogan et al. (2005) analysis, variability will not impact our optical depth calculations, because (1) the continuum appropriate for each epoch was used in the optical depth calculations, (2) amplitude self-calibration solutions were never transferred between the epochs, and (3) the intrinsic continuum morphology at 10 mas resolution does not appear to change from epoch to epoch.

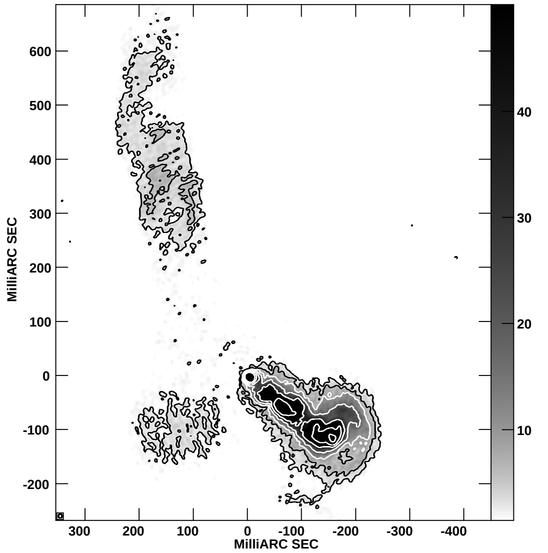

Fig. 1.— The Epoch II (2005) 21 cm continuum image of 3C 147 obtained with the VLBA and phased VLA. The CLEAN beam is 7.6 mas × 7.1 mas at a position angle of −15°. The rms noise level is 0.5 mJy beam^{-1}, and the contours are set at 0.5 mJy beam^{-1} × −3, 5, 7.07, 10, 14.1, 20, ... The gray scale is linear between 1.5 and 500 mJy beam^{-1}. This image shows the source at the full resolution; for subsequent analysis, the image was convolved to 10 mas resolution. The origin is at (J2000) $05^{\mathrm{h}}\,42^{\mathrm{m}}\,36\overset{\mathrm{s}}{.}1379$ $+49^\circ\,51'\,07\overset{\prime\prime}{.}234$.

The flux density in our image is 18 Jy. The VLA Calibrator Manual lists of flux density of 22.5 Jy, indicating that our observations have recovered 80% of the source's total flux density.

3.2. H I Line Profile

Figure 2 shows the average optical depth profile from the new observation of 2005. Even with its relatively high latitude ($b = +10^\circ$), the profile is complex, making it similar to 3C 138 (Brogan et al. 2005). Our profile is in good agreement with previously published profiles (Kalberla et al. 1985; Faison & Goss 2001), and the difference between the line profiles from the two epochs shows only modest variations. Like Faison & Goss (2001), we shall restrict our atten-

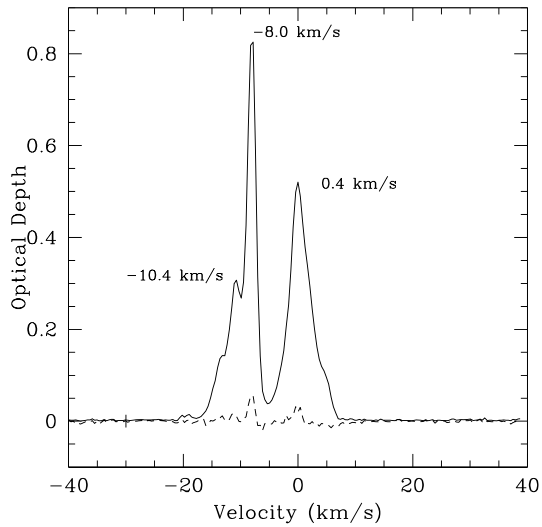

Fig. 2.— The solid line shows the average H I optical depth profile toward 3C 147 from Epoch II (2005). The dotted line shows the difference between the line profiles from the two epochs. Also marked are the three significant velocity components at which further optical depth analysis is performed (viz. Table 2).

tion to the three most prominent velocity components, those with approximate central velocities of −10.4, −8.0, and 0.4 km s^{-1} (see below).

Faison & Goss (2001) have discussed the difficulties with assessing the distance to the absorbing gas. Under the simple assumption that all H I gas is confined to a 100 pc thick layer, the absorbing gas must be within 0.6 kpc. However, the kinematic distance to the gas causing the $-8\,\mathrm{km\ s}^{-1}$ absorption is uncertain, with distances as large as 1.1 kpc allowed. As a nominal value, we adopt the conversion that our resolution of 10 mas corresponds to a linear distance of 7.5 AU ($1\,\mathrm{mas} = 0.75\,\mathrm{AU}$), implying a distance of 750 pc to the gas, though differences of as much 50% are possible.

For subsequent analysis, we fit the 2005 epoch optical depth line cube by gaussian components, using the profile of Figure 2 as an guide to initial values for the component parameters. For the fitting, we focussed on the three significant components identified. The fitting was done on a pixel-by-pixel basis, with an independent three-component fit for each pixel. Table 2 summarizes results of the fits, *averaged* over the face of the the source. Guided by the results of the fitting from the 2005 epoch, a similar fitting was performed for the 1998 epoch.

3.3. Small-Scale Structure

Figures 3 and 4 show *column density fluctuation* images at the two epochs for the three different velocity components. From the gaussian fits, column density images were constructed from the fitting results by multiplying the maximum optical depth by the velocity width ($N_{\mathrm{H\,I}}/T_s \propto \tau\sigma_v$, see below regarding the spin temperature T_s). In order to highlight fluctuations, the average column density from the 2005 epoch across the face of the source was subtracted from these column density images to produce the *column density fluctuation* images. The signal-to-noise is not uniform across the face of the source, and tends to decrease near the edges. In order to aid in assessing the reality of features, Figures 3 and 4 also show the column density fluctuation signal-to-noise ratio images.

We show column density fluctuation images, in contrast to Brogan et al. (2005) who showed optical depth channel images. For 3C 147, analysis of the column density fluctuations is required because the velocity field of the absorping gas appears to change somewhat within each velocity component. For 3C 138, Brogan et al. (2005) compared the optical depth channel images at different velocities and concluded that any velocity field fluctuations were negligible, in contrast to the situation for 3C 147. Also, in converting to column density, we assume a uniform spin temperature of the gas of $T_s = 50$ K (Heiles 1997). Unlike 3C 138 which was part of the Millennium Arecibo 21 cm Survey (Heiles & Troland 2003), 3C 147 is outside the Arecibo declination range so that there is less direct information about the absorbing gas along this line of sight.

Figures 5–8 show cuts through the column density fluctuation images. In all cases, spatially significant changes in the column density between the two epochs are clearly apparent for all of the H I components, at significance levels exceeding 5σ over most of the face of the source. We have also conducted an analysis in which we consider a constant column density cross-cut to be the null hypothesis. In a χ^2 sense, the null hypothesis can be firmly rejected as typical values, for both epochs

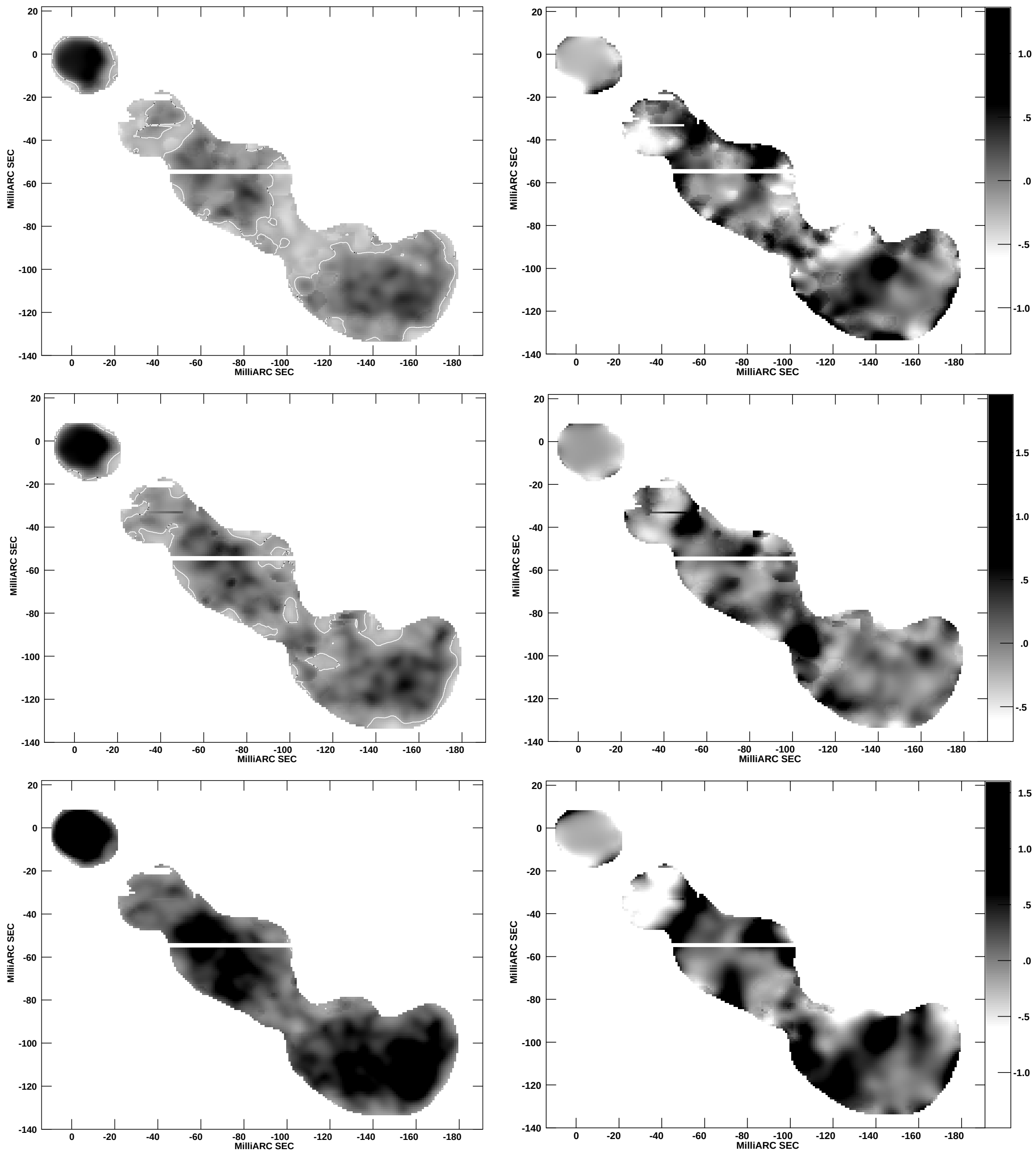

Fig. 3.— Column density *fluctuation* images, for the 1998 epoch (Epoch I), with the average value of the 2005 epoch column density subtracted, $\Delta N_{\rm H\,I}/T_s \propto \int dv\,(\tau - \langle\tau_{2005}\rangle)$. Horizontal white lines are pixels where the gaussian fitting failed to converge. *Left* panels show the signal-to-noise ratio, on a linear scale with the dynamic range restricted to 0–15 and with a single contour showing a signal-to-noise ratio of 5. *Right* panels show the column density fluctuations, on a linear scale. The gray scale bar shows the column density fluctuation, in units of 10^{19} cm^{-2}. (*Top*) Column density fluctuations for $-10.4\,{\rm km\,s^{-1}}$ velocity component in 1998, the 2005 average *optical depth* that was subtracted is $\langle\tau_{2005}\rangle = 0.31$; (*Middle*) Column density fluctuations for $-8.0\,{\rm km\,s^{-1}}$ velocity component in 1998, $\langle\tau_{2005}\rangle = 0.93$; and (*Bottom*) Column density fluctuations for $0.4\,{\rm km\,s^{-1}}$ velocity component in 1998, $\langle\tau_{2005}\rangle = 0.54$.

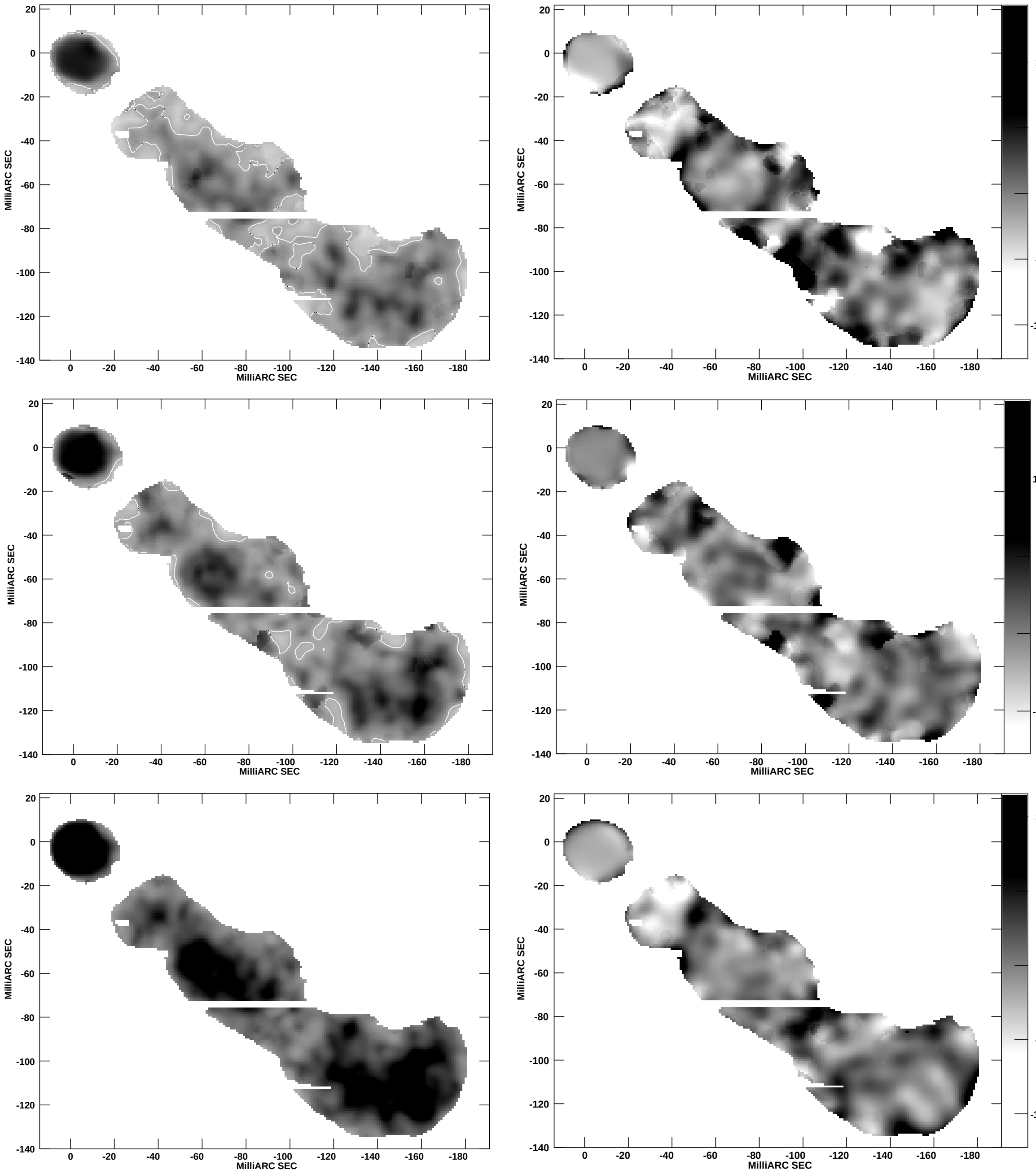

Fig. 4.— Column density fluctuation images, as for Figure 3 but for the 2005 epoch (Epoch II).

TABLE 2
OPTICAL DEPTH PROFILE GAUSSIAN COMPONENT FIT RESULTS

Component	Epoch	Central Velocity (km s^{-1})	Velocity Width (km s^{-1})	Maximum Optical Depth
1	1998	0.4	5.1	0.5
	2005	0.3	4.9	0.5
2	1998	−8.0	1.6	0.8
	2005	−8.0	1.5	0.8
3	1998	−10.4	6.1	0.3
	2005	−10.4	6.2	0.3

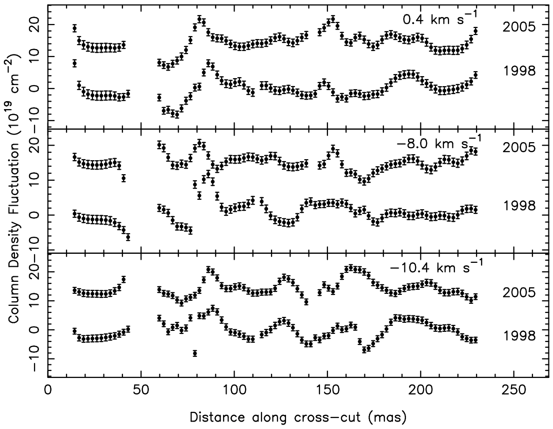

Fig. 7.— Comparison of a cross-cut along the major axis at the two epochs for the three velocity components. For clarity, the 1998 epoch is shifted (by 15×10^{19} cm^{-2}) relative to the 2005 epoch. For both epochs, a spin temperature $T_s = 50$ K is assumed. Also shown are uncertainties ($\pm 2\sigma$), although in many cases they are only slightly larger than the symbol size. Further, because the restoring beam can induce correlations, we plot only every fifth datum. The major axis illustrated is the central of the three in Figure 5.

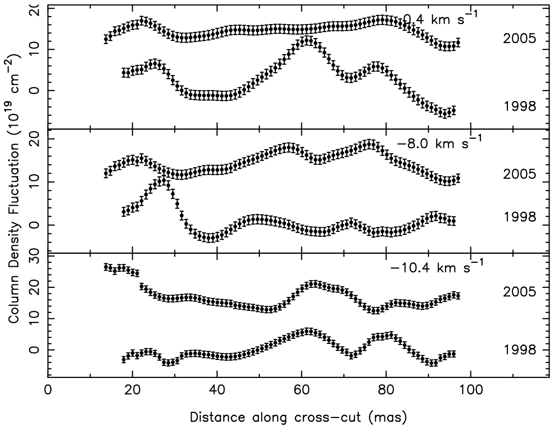

Fig. 8.— As for Figure 7 (and Figure 6), but for a minor axis slice.

and all velocity components, are $\chi^2 \sim 10$ (reduced χ^2). Typical angular scales for column density variations are approximately 15 mas, corresponding to a linear scale of approximately 10 AU.

Brogan et al. (2005) discussed the possible systematic effects that might affect the extraction of reliable optical depth or column density variations from dual-epoch imaging such as presented here. We do not repeat their discussion, but consider many of the same issues and conclusions to hold. Namely, while small differences in the images from epoch to epoch may be due to the details of the observations and data reduction (e.g., spatial frequency or *u*-*v* coverage, slight differences in the imaging), a number of steps were taken during the analysis in an effort to minimize the differences between the epochs, and the column density variations are significant.

The column density fluctuations in Figures 5–7 correpond to peak-to-peak optical depth variations as large as $\Delta\tau \approx 0.7$, and typical optical depth variations on scales of approximately 15 mas ranges from 0.1–0.3. The associated uncertainties in the optical depth are $\sigma_\tau \approx 0.07$, implying significant variations at the 3σ level, and the column density cross-cuts indicate variations at even higher significance are present. Fur-

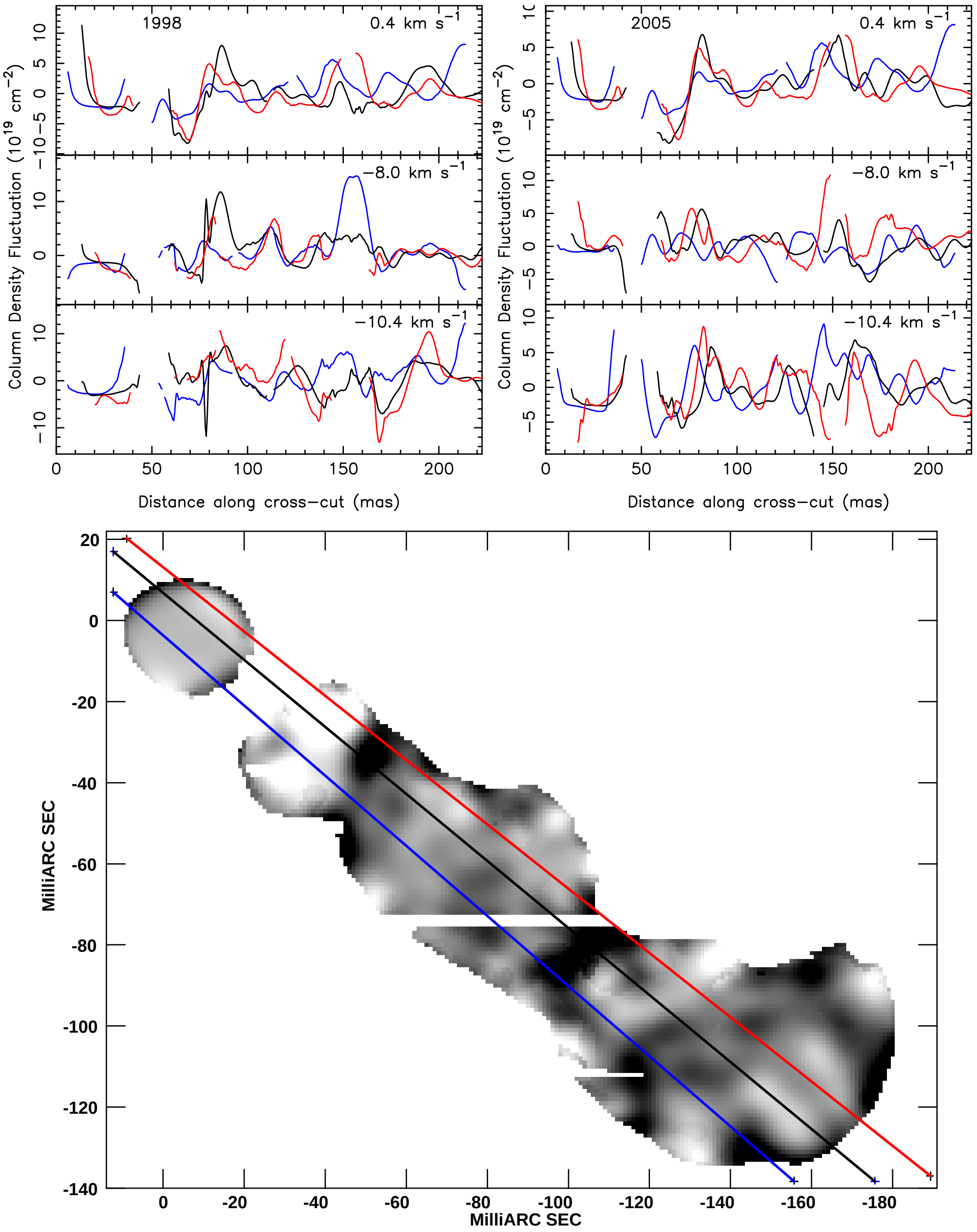

Fig. 5.— (*Top Left*) Cross-cuts taken approximately along the major axis showing the column density fluctuations for the 1998 epoch. (*Top Right*) Cross-cuts taken approximately along the major axis showing the column density fluctuations for the 2005 epoch. (*Bottom*) Illustration showing where the cross cuts were taken taken, with the column density fluctuations from the 0.4 km s^{-1}, 2005 epoch shown for reference.

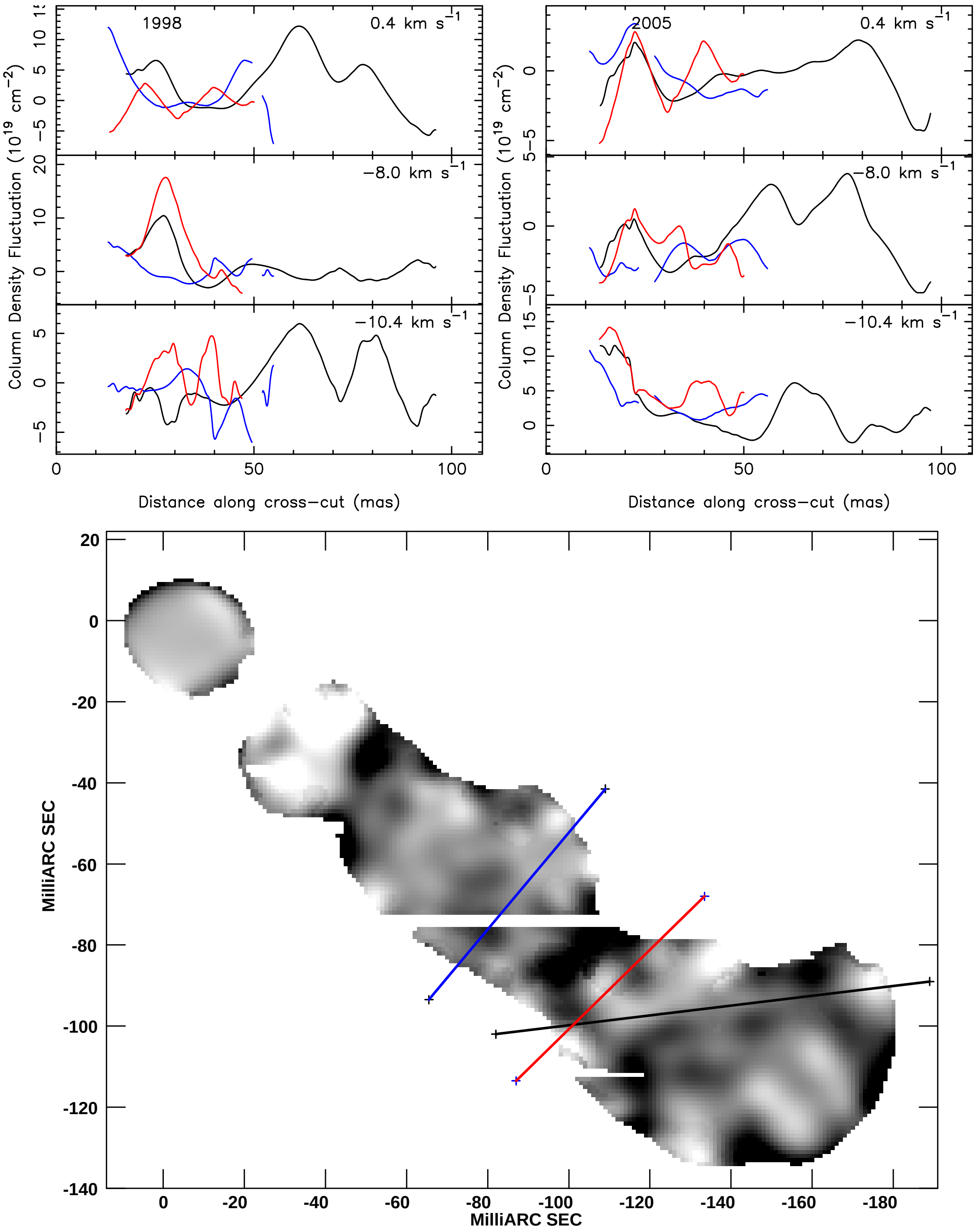

Fig. 6.— As for Figure 5, but for the minor axis.

ther, the magnitude of the variations is approximately correlated with the strength of the average H I absorption toward 3C 147, in that the largest variations are observed at -8.0 km s^{-1}, followed by 0.4 km s^{-1}, with the smallest variations at -10.4 km s^{-1} (cf. Figures 2 and 5–8).

The opacity variations toward 3C 138 show changes that are consistent with motion of structures across the line of sight (Brogan et al. 2005), though there is considerable uncertainty with making these identifications (as they discuss). Possible motions of structures across the line of sight toward 3C 147 are also visible in the cross-cuts. Examples of such motions include the features at distances between 50 and 100 mas (Figures 7). Caution in interpreting these features as arising from motions is clearly warranted, however, given that we have only two epochs. Nonetheless, typical position shifts appear to be of the order of 5 mas. Over the 7 yr interval between observations, the implied proper motion is just under 1 mas yr^{-1}, equivalent to a velocity of order 3 km s^{-1}, at a distance of 750 pc. For comparison, and recognizing that there is considerable uncertainty in these comparisons, Brogan et al. (2005) find larger values for the apparent velocities of structures toward 3C 138 (≈ 20 km s^{-1}).

One of the motivations for undertaking these observations was to assess whether the optical depth variations, both spatial and temporal, found by Brogan et al. (2005) toward 3C 138 indicated that the line of sight to that source was in some sense "special" or anomalous. Comparison of Figures 3 and 4 and Figures 5–8 with the corresponding ones from Brogan et al. (2005) show that they are qualitatively similar, with clearly significant opacity or column density variations occurring both in space and time.

Quantitatively, there are modest differences in the opacity/column density variations between 3C 147 and 3C 138. We estimate that the typical angular scale of opacity variations is 15 mas (≈ 10 AU), as opposed to about 50 mas (≈ 25 AU) toward 3C 138, though the linear scales are comparable. The magnitude of the variations toward 3C 147 also seems somewhat smaller. Optical depth changes (both in space and time), and corresponding column density fluctuations, are a factor of a few to several larger for 3C 138—optical depth changes of 0.4 and larger ($> 10^{20}$ cm^{-2}) for 3C 138 vs. optical depths typically not exceeding 0.3 ($\sim 5 \times 10^{19}$ cm^{-2}) for 3C 147.

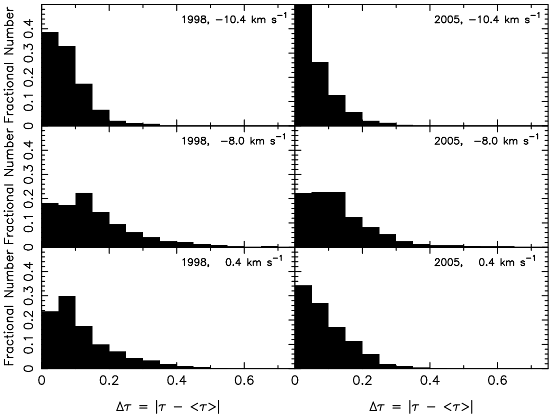

Fig. 9.— Fractional number of pixels in an optical depth channel image as a function of the optical depth variation $\Delta\tau \equiv |\tau - \langle\tau\rangle|$. *Left* panels show the first epoch (1998), and *right* panels show the second epoch (2005). (*Top*) -10.4 km s^{-1}; (*Middle*) -8.0 km s^{-1}; and (*Bottom*) 0.4 km s^{-1}.

3.4. Small-Scale H I Covering and Filling Factors

Brogan et al. (2005) used their observations of 3C 138 to conclude that the (two-dimensional) *covering factor* of small-scale H I opacity variations was about 10%, from which they inferred a three-dimensional filling factor of probably less than 1%. Although the optical depth variations appear qualitatively similar for lines of sight toward 3C 138 and 3C 147, we have repeated their analysis in order to determine the covering and filling factors for the line of sight to 3C 147.

Figure 9 shows the fractional number of pixels in a optical depth channel image for the three different velocities at both epochs. Most of the opacity variations are at a level less than about 0.2 in optical depth, and we do not consider them significant. Restricting to optical depth variations larger than approximately 0.2 ($\approx 3\sigma$), most of the covering fractions are about 10%, ranging from a low value of a few percent to a high exceeding 25%.

While we have decomposed the optical depth profile into gaussian components, our decomposition is likely not unique and we fit only for three components, whereas Figure 2 clearly shows that there are could be more components. Thus, a plausible upper limit to the volume filling factor of the small-scale absorbing gas is obtained by assuming that there are multiple components, each of which contributes equally. We obtain an upper limit of 1%, a value which, as Brogan et al. (2005) emphasize, is not directly measurable.

4. Discussion and Conclusions

We have presented two epochs of observations of the H I optical depth across the face of the source 3C 147 on scales of approximately 10 mas. The motivation for these observations was assessing whether spatial and temporal H I opacity variations found in multi-epoch observations of 3C 138 by Brogan et al. (2005) were in some sense "special" or anomalous.

We find qualitatively similar opacity and column density variations toward 3C 147 as were found toward 3C 138. Quantitatively, the variations toward 3C 147 appear to be somewhat smaller in angular scale (15 mas vs. 50 mas) and smaller in magnitude (by a factor ~ 5). While the typical angular scale of the variations toward 3C 147 appears smaller, the absorbing gas may be more distant than that causing the absorption toward 3C 138 (§2). If so, the resulting linear scales are comparable (10 AU for 3C 147 vs. 25 AU for 3C 138), though the uncertainties are large.

Further similarities are observed in the covering and filling factors of the small-scale absorbing gas toward both sources. For both lines of sight, the covering factor appears to be approximately 10%, and the volume filling factor, while not measured directly, has a plausible upper limit of 1% (and potentially much less).

Both 3C 138 and 3C 147 display significant H I opacity variations across their faces, implying variations within the ISM on scales of about 10 to 50 AU over path lengths ranging from 100 to 1000 pc. Using MERLIN, Goss et al. (2008) also have resolved significant H I opacity variations across the faces of 3C 111, 3C 123, and 3C 161, implying structure on scales of 50 to 500 AU. We conclude that the conditions that cause such small-scale variations are fairly widespread within the Galactic ISM. The reason that so few other sources display such small-scale opacity variations is likely to be, as Brogan et al. (2005) discuss, that few sources other than 3C 138 and 3C 147 have the combination of angular extent and surface brightness required to conduct these observations. One unfortunate implication of this conclusion is that milliarcsecond-scale H I observations of other sources will largely not be useful for probing the small-scale structure without a significant increase in sensitivity. One possible target, particularly with the existing High Sensitivity Array (HSA),[1] may be 3C 380.

In one aspect, however, the lines of sight to 3C 147 and 3C 138 do differ. For the 3C 138 analysis, Brogan et al. (2005) used optical depth velocity channel images whereas, for 3C 147, we fit the optical depth line cube with gaussian components and used the resulting column density images. This difference in approach was motivated by the velocity structure that was apparent within an H I component in the 3C 147 optical depth line cube.

We have not been able to find a ready explanation for this difference. Both sources are seen toward the Galactic anticenter, with Galactic coordinates (longitude, latitude) of ($161\overset{\circ}{.}7$, $10\overset{\circ}{.}3$) for 3C 147 and ($187\overset{\circ}{.}4$, $-11\overset{\circ}{.}3$) for 3C 138, respectively. To first order, the lines of sight to both cut almost perpendicular to the Perseus spiral arm. Further, were velocity crowding the explanation, it would seem that that should be more of an issue for 3C 138 than for 3C 147. We have also consulted the WHAM Hα survey and the Green supernova remnant (SNR) catalog (Green 2006), reasoning that Hα and SNRs might serve as a tracers of turbulence injected by winds or explosions from massive stars. There are no obvious indications that the line of sight to 3C 147 should be affected any such turbulence—indeed a comparison of the 3C 138 and 3C 147 lines of sight suggest that the line of sight to 3C 138 would be *more* likely to be the one that would display any such evidence of turbulence.

An alternate possibility is that the kinematic differences between these two lines of sight reflect small-scale features, and possibly the past history of the gas. Kalberla et al. (1985) imaged the H I emission around the line of sight toward 3C 147 at $1'$ resolution (≈ 1 pc linear scale). They found a series of filaments and small clumps of H I emission, and they were able to associate at least some of the absorption features with small emission clumps. The amount of small-scale structure (in H I emission) toward 3C 147 is not generally observed in the on-going GALFA H I survey at Arecibo. Further, Kalberla et al. (1985) find that a large fraction ($\sim 80\%$) of the H I in emission in the direction of 3C 147 has a temperature of 500–2000 K. At this temperature, the gas would be thermally unstable. While the warm H I is not responsible for the absorption, the possibility that this line of sight contains thermally unstable H I is consistent with a scenario in which the microphysics, and potentially the past history of the gas, leads to kinematic variations within an H I absorption component.

---

[1] The VLBA combined with other large aperture telescopes such as the phased VLA, the Green Bank Telescope, Arecibo, or the 100-m Efflesberg telescope.

Kalberla et al. (1985) also suggested a relative distance ordering of the gas. Comparison of the opacity variations (Figures 5–8) suggests that the opacity variations are smallest in amplitude for the -10.4 km s^{-1} velocity component and increase in magnitude for the 0.4 km s^{-1} and the -8.0 km s^{-1} velocity components. One interpretation is that the opacity variations result from structures of essentially constant size, which are comparable to or smaller than the equivalent linear size of our beam ($\sim$ 10 AU). If this were the case, we could obtain a relative distance ordering of the gas, with the -8.0 km s^{-1} material being the nearest, followed by the 0.4 km s^{-1} material, and the -10.4 km s^{-1} material being the most distant. An alternate interpretation (see above) would attribute these differences to the history of exposure of the gas to shocks or other interstellar disturbances. Whichever is the case, there is clearly significant structure on large scales ($\sim$ 1 pc), suggesting that such structure could persist to smaller scales. The combination of VLBA and VLA data (as well as potentially MERLIN data) might be able to explore the connection between the small- and large-scale opacity variations.

Bregman et al. (1983) have set an upper limit (3σ) on the magnetic field toward 3C 147 of $B_{\parallel} < 50\,\mu$G, based on Zeeman effect measurements in H I spectra. Under the standard assumption that discrete H I structures require densities $n \sim 10^5$ cm^{-3} (Heiles 1997), with a typical velocity width of $v \approx 3\,\mathrm{km\ s}^{-1}$ (Figure 2 and Table 2), one concludes that magnetic and turbulent equipartition requires a magnetic field strength of order 400 μG, well above the observed upper limit. As for the optical depth variations toward 3C 138 (Brogan et al. 2005), the optical depth variations cannot be in magnetic and turbulent equilibrium, unless there is significant blending and dilution of the magnetic field on the angular scales over which the Zeeman effect measurements were made.

Our observations of 3C 147 do not produce any new constraints on the nature of the small-scale structures vis-a-vis whether they represent “statistical” fluctuations (e.g., Deshpande 2000), “non-equilibrium” physical structures (e.g., Jenkins & Tripp 2001; Hennebelle & Audit 2007), or discrete “tiny scale atomic structures” (Heiles 1997). While the level of opacity variations toward 3C 147 are lower than those toward 3C 138, we believe that this lower level can be accommodated easily within any of these scenarios. A wide range of opacity variations might be expected if these result from non-equilibrium processes, particularly because the level of opacity variations could depend upon the history of the gas. Also, as Brogan et al. (2005) note, the predicted level of opacity variations within a statistical description depends sensitively upon the assumed spectral index of the underlying power law; within the current uncertainties for this spectral index, a large range of opacity variations is allowed.

What would be required in order to place significant constraints on these small-scale opacity variations? Ideally, one should monitor the same volume of gas and determine how the structures evolve. In the most simple comparison, discrete structures should show only linear motion across the line of sight, while fluctuations or non-equilibrium physical conditions might also cause the appearance of the opacity variations to change significantly.

The elapsed times between observations presented here and those in Brogan et al. (2005) range from 3 to 7 yr. These intervals are only a few percent of the estimated time for discrete structures to change substantially ($\approx$ 500 yr, Heiles 2007). However, on milliarcsecond scales, the line of sight to 3C 147 effectively samples a volume through the Galaxy (Marscher et al. 1993; Dieter-Conklin 2009). The Sun’s velocity through space causes this volume to move between our observing epochs (Figure 10), in addition to any

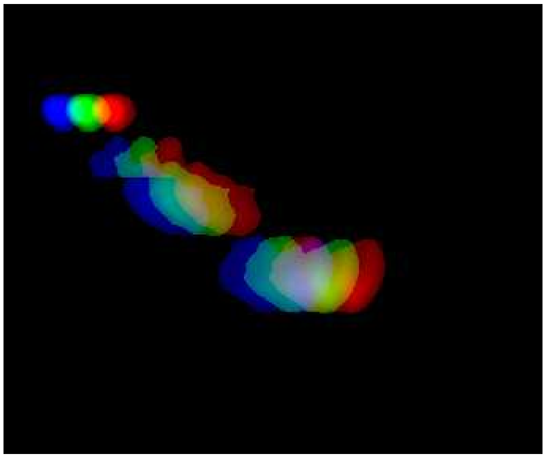

Fig. 10.— An illustration of the different volumes of the Galaxy sampled by multi-epoch VLBI observations. The distance to the absorbing gas is assumed to be 750 pc, the space velocity of the Sun is assumed to be 30 km s^{-1}, and the gas is assumed to be stationary. The resulting effective proper motion is 8.4 mas yr^{-1}; a smaller assumed distance for the gas would result in a larger proper motion while a smaller space velocity for the Sun would result in a smaller proper motion. Shown is the apparent position of the source at three hypothetical epochs, each separated by 3 yr, comparable to the typical separation in epochs for the existing multi-epoch VLBI H I absorption observations. (Epoch I is red, Epoch II is green, and Epoch III is blue.) The white areas indicate the *only* sampled volumes of gas common to all three epochs.

motion that the gas itself might have. A simple estimate of the Sun's motion suggests that an entirely new volume through the Galaxy could be sampled on time scales of approximately 3 yr. That is, in the typical interval between VLBI observations, essentially an entirely new volume of the Galaxy is sampled by the line of sight.

Consequently, we also conclude that the time sampling of the existing multi-epoch VLBI observations has been too coarse to distinguish between the various models for the small-scale opacity variations. Ideally, one would like to monitor the same volume of gas, to determine if the opacity variations appear to be simply in motion or also changing in appearance. We estimate that, for either 3C 138 and 3C 147, an appropriate sampling interval is no longer than about 9 months, with even more rapid sampling desirable.

We thank N. Dieter-Conklin for helpful discussions on the motion of the lines of sight through the Galaxy. We thank J. Dickey, the referee, who made insightful comments that we believe improved the analysis presented here. The Wisconsin H-Alpha Mapper is funded by the National Science Foundation. This research has made use of the SIMBAD database, operated at CDS, Strasbourg, France. This research has made use of NASA's Astrophysics Data System. The National Radio Astronomy Observatory is a facility of the National Science Foundation operated under cooperative agreement by Associated Universities, Inc. Basic research in radio astronomy at the NRL is supported by 6.1 NRL Base funding.

REFERENCES

Bregman, J. D., Forster, J. R., Troland, T. H., Schwarz, U. J., Goss, W. M., & Heiles, C. 1983, A&A, 118, 157

Brogan, C. L., Zauderer, B. A., Lazio, T. J., Goss, W. M., DePree, C. G., & Faison, M. D. 2005, AJ, 130, 698

Dieter-Conklin, N. 2009, AJ, submitted

Davis, R. J., Diamond, P. J., & Goss, W. M. 1996, MNRAS, 283, 1105

Deshpande, A. A. 2000, MNRAS, 317, 199

Deshpande, A. A., Dwarakanath, K. S., & Goss, W. M. 2000, ApJ, 543, 227

Diamond, P. J., Goss, W. M., Romney, J. D., Booth, R. S., Kalberla, P. M. W., & Mebold, U. 1989, ApJ, 347, 302

Dieter, N. H., Welch, W. J., & Romney, J. D. 1976, ApJ, 206, L113

Faison, M. D., & Goss, W. M. 2001, AJ, 121, 2706

Faison, M. D., Goss, W. M., Diamond, P. J., & Taylor, G. B. 1998, AJ, 116, 2916

Frail, D. A., Weisberg, J. M., Cordes, J. M., & Mathers, C. 1994, ApJ, 436, 144

Goss, W. M., Richards, A. M. S., Muxlow, T. W. B., & Thomasson, P. 2008, MNRAS, in press

Green D. A., 2006, “A Catalogue of Galactic Supernova Remnants (2006 April version),” `http://www.mrao.cam.ac.uk/surveys/snrs/`

Heiles, C. 2007, in SINS—Small Ionized and Neutral Structures in the Diffuse Interstellar Medium, eds. M. Haverkorn & W. M. Goss (ASP: San Francisco) p. 3

Heiles, C. 1997, ApJ, 481, 193

Heiles, C. & Troland, T. H. 2003, ApJS, 145, 329

Hennebelle, P., & Audit, E. 2007, A&A, 465, 431

Jenkins, E. B. 2004, Ap&SS, 289, 215

Jenkins, E. B. & Tripp, T. M. 2001, ApJS, 137, 297

Johnston, S., Koribalski, B., Wilson, W., & Walker, M. 2003, MNRAS, 341, 941

Kalberla, P. M. W., Schwarz, U. J., & Goss, W. M. 1985, A&A, 144, 27

Marscher, A., Moore, E., & Bania, T. 1993, ApJ, 419, L101

Polatidis, A. G., Wilkinson, P. N., Xu, W., Readhead, A. C. S., Pearson, T. J., Taylor, G. B., & Vermeulen, R. C. 1995, ApJS, 98, 1

Readhead, A. C. S., & Wilkinson, P. N. 1980, ApJ, 235, 11

Stanimirović, S., Weisberg, J. M., Hedden, A., Devine, K. E., & Green, J. T. 2003, ApJ, 598, L23

Zhang, F. J., Akujor, C. E., Chu, H. S., Mutel, R. L., Spencer, R. E., Wilkinson, P. N., Alef, W., Matveyenko, L. I., & Preuss, E. 1991, MNRAS, 250, 650

This 2-column preprint was prepared with the AAS LaTeX macros v5.2.